Pergamon

*Journal of Atmospheric and Terrestrial Physics*, Vol. 57, No. 12, pp. 1415–1432, 1995

0021-9169/95 $9.50+0.00

0021-9169(94)00141-3

# Ionospheric changes in response to IMF variations

A. T. Karpachev, G. F. Deminova and S. A. Pulinets

Institute of Terrestrial Magnetism, Ionosphere and Radiowave Propagation, Russian Academy of Sciences (IZMIRAN), Troitsk, Moscow Region, 142092 Russia

(*Received in final form* 18 *July* 1994; *accepted* 4 *August* 1994)

**Abstract**—This paper attempts to summarize the results of investigations of IMF effects on the ionosphere, published mostly in Russian, and to place them in context in up-to-date knowledge of IMF/magnetosphere/ionosphere relationships. Effects of the IMF sector structure and of the IMF $B_z$ component turnings on the ionospheric F-layer are considered, including variations of position of the main ionospheric trough (MIT). The paper includes results of both theoretical calculations and observational data obtained mostly by the Cosmos-900, Intercosmos-19 and Cosmos-1809 satellites at subauroral, middle and low latitudes. The MIT position dependence on longitude has been derived as a background for further study. It has been shown that the nightside winter trough position at the storm growth phase correlates best with $K_p$ index taken with a time delay $\tau$, which is proportional to a disturbance growth rate $\Delta K_p/\Delta t$. The MIT position dependence on $D_{st}$, $B_z$ and $B_y$ is also shown. Two troughs have been found to be formed usually in the storm recovery phase at postmidnight hours: these are the MIT (main ionospheric trough) and RIT (ring ionospheric trough) associated with the DR-current. In general the MIT position's response to $B_z$ southward turnings corresponds well to changes of the auroral diffuse precipitation equatorial edge. For $B_z$ southward turnings the height of the equatorial night-time F-layer lowers, and at equatorial latitudes $f_0F2$ decreases sharply, the latter effect being most pronounced at 03 LT. Large-scale internal gravity waves arriving at equatorial latitudes from the auroral oval cause intensification of the equatorial anomaly, both in daytime and night-time. A schematic pattern of a global ionospheric response to a magnetic disturbance is constructed using as an example the strong storm on 3–4 April 1979.

## 1. INTRODUCTION

The solar wind and IMF parameters control the magnetosphere's geometry and the energy input into it. The IMF $B_z$ component plays the key role, since the degree of reconnection between the geomagnetic field and IMF, and consequently the energy input into the magnetosphere, depend on $B_z$ orientation and magnitude. During solar maximum periods about 90% of major magnetic storms are caused by large southward $B_z$ turnings which in turn are connected with interplanetary shocks (Tsurutani *et al.*, 1990). Energy of order $10^{16}$ J is introduced into the magnetosphere during a storm; the day cusp location changes, as well as the inner edge of the plasmasheath, the plasmapause, etc. The magnetospheric variations are reflected onto the coupled ionospheric structures such as the positions of the cusp projection, the auroral oval as a whole, the electron density trough, the subauroral $T_e$ peak, etc.

Energy from the solar wind having velocity $V_{sw}$ is introduced into the magnetosphere in the form of the electric field of magnetospheric convection $E_m \sim B_z V_{sw}$ and precipitating particle fluxes which are also controlled by the magnitude of $B_z$. The latter is shown most clearly by Brautigam *et al.* (1991) (see Fig. 1). The flux of particles increases with $B_z$ not only when $B_z$ is negative but under large positive values of $B_z$ too. The level of magnetic disturbances which is

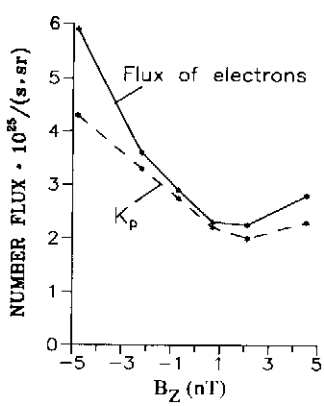


Fig. 1. Variations of $K_p$ index and total electron flux into both auroral ovals (obtained from DMSP satellite data) as a function of the IMF $B_z$ component (after Brautigam *et al.*, 1991).

characterized by the planetary $K_p$ index grows in both cases too. The solar wind energy, which is mainly put into the high-latitude region, is then dissipated by several mechanisms (electric field variations, Joule heating, wave disturbances, etc.) through the ionosphere. So the dynamics of not only the high-latitude ionosphere but of the ionosphere as a whole are controlled directly or indirectly by the $B_z$ component of IMF. The other two components of IMF, namely $B_x$ and $B_y$, control the IMF sector structure (sunward or antisunward). Their variations result in changes of the magnetosphere configuration even at quiet periods. For the ionosphere this effect is reflected as asymmetries of the polar convection system and a displacement of the auroral oval as a whole with respect to the magnetic pole.

Many papers, including excellent reviews, have been devoted to various manifestations of IMF control of ionospheric behaviour. The present review does not intend to consider all aspects of this problem; its purpose is mainly to review the studies dealing with $N_e$ and $T_e$ variations conducted in Russia derived from data of the Cosmos-900 and Intercosmos-19 satellites which operated during high solar activity (1977–1981), and to set them in context in the general up-to-date picture of ionospheric responses to IMF variations.

## 2. HIGH LATITUDES

### 2.1. *The auroral oval dynamics*

High-latitude ionospheric variations are strongly determined by the dynamics of the auroral oval and the main ionospheric trough (MIT) adjacent to it. Variations of the auroral oval boundaries were intensively studied on the basis of the soft particle precipitation data from DMSP satellites. We consider the equatorward boundary of the auroral diffuse precipitation (EBDP) which determines the poleward wall of the trough. The dayside oval position variations (dayside cusp) follow most closely (with correlation coefficient $r = 0.85$) the $B_z$ variations of the IMF, especially variations with short periods and small delays ($\tau \leqslant 0.5$ *h*) (Carbary and Meng, 1988). The night-side oval displacement towards the equator is related to the $B_z$ equatorward turning too but in this case the correlation is not so good, especially during the recovery phase of the storm ($r = 0.4$ 0.6) and the delay time is larger (up to 2–3 h) (Meng, 1983). The maximum equatorward displacement is reached during night-time for a maximum of the auroral activity (AE index), (Makita *et al.*, 1985). Correlation with the $D_{st}$ index is observed too, especially for short-period variations, but in general the $D_{st}$ variations are delayed. The best correlation for night-time conditions is reached for $K_p$ index values taken 3–6 h before the considered time (Soloviov *et al.*, 1989). In the same way the correlation with $B_zV_{sw}$ is a maximum when the maximum value of $B_zV_{sw}$ is taken for the previous 6 h (Nakai and Kamide, 1983). The EBDP variations during a storm have an exponential shape with $\tau \sim 45$ min during the growth phase and $\tau \sim 8$ h during the recovery phase (Nakai *et al.*, 1986). These features will be compared below with the similar characteristics for the main ionospheric trough directly adjoining the EBDP.

### 2.2. *Trough position variations with longitude*

It is well known that the poleward wall of the MIT is formed by the soft auroral diffuse precipitation and its variations should follow, in general, the variations of the EBDP position. But in the morning sector this tight relationship is often broken: noticeable precipitation may be absent there (Rodger *et al.*, 1986) and a two-step structure in $N_mF2$ at the poleward wall itself may be observed (Khalipov *et al.*, 1985). The relationship between variations in the EBDP position and the trough minimum position seems to be still more complex, because the trough minimum position may in addition vary with longitude, up to 10–11° in latitude, for the same local time and magnetic activity level (Deminov and Karpachev, 1986). The EBDP seems also to vary its position with longitude (although with less amplitude), but there is only one study concerning this interesting problem (Meng, 1979). Investigation of longitudinal variations in the trough minimum position, which began using Intercosmos-19 satellite data (Deminov and Karpachev, 1986), was continued using a large amount of data obtained from the Cosmos-900 satellite (Afonin *et al.*, 1992; Deminov *et al.*, 1992b; Karpachev *et al.*, 1994). The amplitude of the longitudinal variations is comparable with the MIT position variations during a moderate storm and so they should be taken into account when analysing changes of the high latitude ionosphere.

In Fig. 2 the longitudinal variations in the trough minimum position are shown for the Northern hemisphere (a) and for the Southern hemisphere (b), for local winter and equinoxes in both hemispheres. The data are taken from Cosmos-900 satellite local density measurements at altitudes 350–500 km for quiet ($K_p \leqslant 3$) night-time conditions during a high solar activity period 1977 1979. Experimental data are shown by dots and approximation curves by solid lines for the winter (Afonin *et al.*, 1992) and dashed

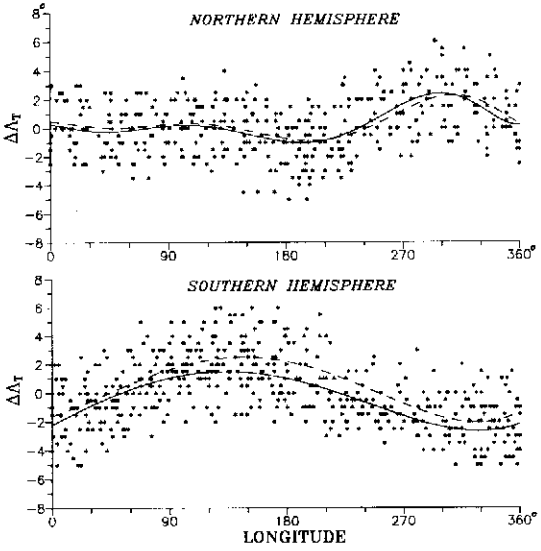


Fig. 2. Longitudinal variations of the night-time trough minimum position $\Delta\Lambda_T$ in the Northern and Southern hemispheres for quiet ($\bar{K}_p \simeq 2$) winter and equinox conditions (dots). $\Delta\Lambda_T = \Lambda_T^{expr} - \Lambda_T^{mod}$, where $\Lambda_T^{expr}$ are the data from the Cosmos-900 satellite and $\Lambda_T^{mod}$ are calculated from the model Kohnlein and Raitt (1977). The solid curve is the best fit for winter and the dashed curve for equinox conditions.

lines for equinoxes (Karpachev *et al.*, 1994). In Fig. 2 $\Delta\Lambda_T = \Lambda_T^{expr} - \Lambda_T^{mod}$, where $\Lambda_T^{expr}$ are the Cosmos-900 satellite data and $\Lambda_T^{mod}$ are calculated from the model (Kohnlein and Raitt, 1977) for specific MLT and $K_p$. In particular $\Lambda_T^{mod} \simeq 61°$ for 00 MLT and $K_p \simeq 2$ (the mean value of $K_p$ for the whole amount of the data). More than 800 cases have been analysed (365 cases for the Northern hemisphere and 455 for the Southern hemisphere). The standard deviation $\sigma$ is approximately equal to 1.8° for all seasons and both hemispheres. The scatter may be decreased, with $\sigma \simeq 1.3°$, by means of more careful data processing (Karpachev *et al.*, 1994) and then the correlation coefficient for the best fit line is equal to 0.75–0.80 for the Southern hemisphere and ~0.65 for the Northern hemisphere. We emphasize that, in this connection, in the Southern (Northern) hemisphere, the trough is always, under otherwise equal conditions, near longitude 150° (315°) situated poleward than near longitude 330° (210°).

As one can conclude from Fig. 2 the longitudinal variations are different for the two hemispheres. This can be explained by the different configuration of the terrestrial magnetic field in the different hemispheres (Deminov and Karpachev, 1986). The trough position variations with longitude could be expressed in a simple way by the first harmonic in the Southern hemisphere almost without loss of precision:

$$\Lambda\Lambda_T^S = A\cos(\lambda + 30°) \quad (1)$$

and by two harmonics in the Northern hemisphere:

$$\Delta\Lambda_T^N = \frac{A}{2}[\cos(2\lambda - 50°) - \cos(\lambda + 40°)] \quad (2)$$

The amplitude of the longitudinal effect decreases when the magnetic disturbance grows: $A = A_0(1 - 0.1K_p)$, where $A_0 = 5°$–$6°$ (Deminov *et al.*, 1992b). The winter trough on average is situated more equatorward at all longitudes than in the equinox period. But during disturbed conditions the situation is opposite: the winter trough was found on average 1° poleward of its equinox position. This effect is not so strong but it entirely coincides with the seasonal variations of the subauroral $T_e$ peak position which was revealed from the DE-2 satellite data analysis (Fok *et al.*, 1991) and probably may be explained by $N_e$ seasonal variations in the outer plasmasphere (Karpachev *et al.*, 1994). However, it should be noted that the equatorial boundary of the auroral oval in winter is more poleward (approximately by 2°) than in summer (Kamide and Winningham, 1977). This is connected with the seasonal variations of the dipole inclination angle, which changes the degree of interaction of the Earth's magnetic field with the $B_z$ component of the IMF. Thus the displacement between the EBDP and the trough minimum is expected to decrease when passing from winter conditions to equinoctial ones (and then to summer ones) under low magnetic activity conditions. This fact needs to be verified by means of simultaneous observations of both boundaries.

### 2.3. *Statistical dependence of trough position on* $K_p$ *index*

Taking into account longitudinal variations in the trough position one can try to determine more accurately the dependence of the trough position on the $K_p$ index. For this purpose Cosmos-900 satellite data were used for equinox and local winter conditions in both hemispheres. All the three phases of intense disturbances ($K_p \geqslant 4$): growth phase, main phase maximum, and recovery phase were analysed separately, as well as prolonged ($\geqslant 24$ h) quiet ($K_p \leqslant 2$) periods. Longitudinal variations were taken into account according to expressions (1), (2) and $A = A_0(1 - 0.1K_p)$. All the data are reduced to midnight according to the expression $\Delta\Lambda_T = 0.5t$, where local time $t$ is measured from 00 MLT (Kohnlein and Raitt, 1977). Figure 3 shows examples of the data for the storm growth phase (crosses) and recovery phase (squares) (Karpachev, 1993). A second degree poly-

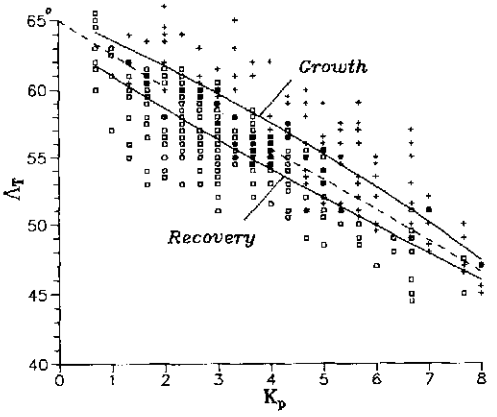


Fig. 3. Variations of the trough minimum position $\Lambda_T$ versus $K_p$ during the growth phase (crosses) and recovery phase (squares) of the intense storms obtained from the Cosmos-900 satellite data. Approximation is presented by solid curves. For the comparison, the regression lines for the maximum main phase of the storms ($K_p \geq 4$) and prolonged quiet periods ($K_p \leq 2$) are shown with dashed lines. The best fit line for all the data together can be presented as $\Delta\Lambda_t = 65^\circ - 2.3K_p$.

nomial was chosen for the best fit line for both phases of the storm. The correlation coefficient is $r \simeq 0.79$ for the growth phase and $r \simeq 0.72$ for the recovery phase. For a storm main phase maximum and for prolonged quiet periods the regression lines are also shown, the data being omitted in order not to overload the Fig. 3. The correlation coefficient is nearly 0.75 for the both these cases. Coefficients in the regression equations for storm main phase maximum, for quiet periods, and for all the data in total are close to each other, and so only the latter is given here:

$$\Lambda_t = 65.0^\circ - 2.3K_p \qquad (3)$$

This equation does not differ significantly from that most often used, $\Lambda_T = 65.2^\circ - 2.1K_p$, which was obtained from ESRO-4 satellite data (Kohnlein and Raitt, 1977). But the difference between the curves for the growth and recovery phases is as much as 3.5°, more than the scatter. Figure 3 shows that, for the growth phase of a disturbance, the trough is often observed at high ('quiet') latitudes even when $K_p$ index has increased up to 4 and even to 6. It is also seen that the minimum latitude of the trough is observed not at the main phase maximum but somewhat later—at the beginning of the recovery phase. During the storm recovery phase, the trough is sometimes observed at latitudes of 51–52° for $K_p \simeq 2$–3, which is 5–6° lower in latitude than for such a level of magnetic activity for the mid-night hours. Also, there is a very dense cloud of data points at latitudes 53–55° for $K_p$ in the interval from 2 to 5 for the storm recovery phase, while from the trough model it follows that $\Lambda_T \sim 57^\circ$ for $K_p = 3.5$. All this shows a strong discrepancy from the curves given in Fig. 3. This discrepancy may be significantly decreased if the $K_p$ value for the preceding 3 h is taken instead of its current value. Thus, the main cause of the discrepancy seems to be a time lag in the trough response to a $K_p$ change for all phases of a storm. This problem is discussed in detail in the next section using a case study.

### 2.4. *Trough dynamics during an intense storm*

Over 30 intense disturbances ($K_p \geq 4$) were analysed carefully for 1978–79 when Cosmos-900 satellite data were available. Three of them, the most typical ones, are shown in Fig. 4 (Deminov *et al.*, 1995). They are plotted from top to bottom as the local time increases (from evening to morning) and as the rate of disturbance intensification $\Delta K_p/\Delta t$ increases (from 0.33 to 0.67) during the storm growth phase. Such an arrangement in Fig. 4 allows us to demonstrate the principal features of the trough dynamics during an intense disturbance. They are as follows. The greater the disturbance growth rate $\Delta K_p/\Delta t$ is, the greater the time delay of the trough response to the $K_p$ variations. Moreover, at the storm initial phase one can observe the slight displacement of the trough in the poleward direction connected with the strong growth of $+D_{st}$ (the bottom panel in Fig. 4). The growth of $+D_{st}$ is caused by the increase in the solar wind pressure, this effect being strongest under $+B_z$ (see e.g. Burton *et al.*, 1975). We should keep in mind that during this time, in accordance with Fig. 1, $K_p$ increases. Then $B_z$ turns south and the trough (with delay $\sim$ 1 h) sharply moves towards the equator. The short-period variations in $D_{st}$ (and $B_z$) are followed exactly by the variations of trough position $\Lambda_T$ as is also observed for the auroral oval (Meng, 1983). So, even when $K_p$ grows strongly, the trough begins to move towards the equator only after $B_z$ has turned southward. Thus, the common statement, that the most dramatic changes in magnetospheric (and ionospheric) structure are observed after $B_z$ turns southward, is valid in this case too. This is also the cause of the variations in time delay of the trough response to $K_p$ index change. Nevertheless, it should be reminded that generally $\Lambda_T$ correlates with $B_z$ less well than with $K_p$, especially for the storm recovery phase. The minimum value of $\Lambda_T$ is usually reached between the $|D_{st}|$ and $K_p$ maxima and also depends on $D_{st}$.

During the recovery phase of a storm one can very often observe two troughs. One of them follows the $K_p$ index variations and is the main ionospheric trough

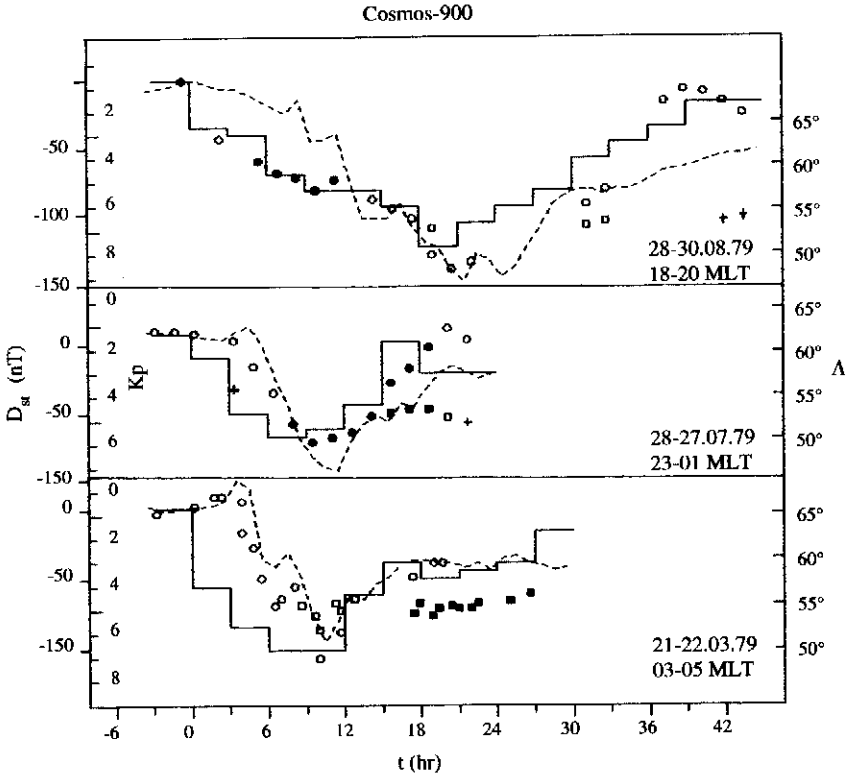


Fig. 4. Variations of the trough minimum positions ($\Lambda_T$) during three magnetic storms. The main ionospheric trough is shown by circles, the ring ionospheric trough by squares, the narrow trough by black symbols, and the peak of $T_e$ without a minimum $N_e$ by crosses. The solid lines show the variations of $K_p$-index, the dashed lines of $D_{st}$. The time origin is the start of the $K_p$-index growth.

by definition (MIT). The second trough is situated equatorward of the MIT. It has very weak response to the $K_p$ index variations and tends towards the latitude of the residual ring current ($\simeq 55°$ Λ). Therefore, this was named the ring ionospheric trough (RIT). It often reveals itself in the form of a narrow trough in the morning sector of local time where it often masks the main ionospheric trough. In the midnight sector one can observe the two troughs simultaneously (if they are sufficiently separated in latitude), but in the evening only the MIT is observed. In Fig. 4, the MIT is marked by circles and the RIT by squares.

Ten, most representative, storms were selected to study the relation between the delay time $\tau$ and storm growth rate $\Delta K_p/\Delta t$ for mid-night and morning hours. The regression line for these shown in Fig. 5 is:

$$\tau = 4.3\Lambda K_p/\Delta t - 0.4 \qquad (4)$$

The correlation coefficient is $r = 0.78$. For comparison, the value of $\tau \simeq 5$ h taken from the Ariel-3 satellite data obtained for 05 LT during the strong storm 25–27 May 1967 (Tulunay and Hughes, 1973) is also shown. In the evening sector (crosses) the dependence in general is similar, but sometimes a sharp increase of delay is observed. This is probably connected with the action of the "polarization jet" (Deminov *et al.*, 1995) which could be observed during the storm growth phase during afternoon and evening hours (Galperin *et al.*, 1973) and which is also known as the sub-auroral ion drift (SAID) (see e.g. Spiro *et al.*, 1979).

We should note that for the average storm growth rate $\Delta K_p/\Delta t \simeq 0.6$ the delay is of order $\tau \simeq 2.2$ h. Now it is clear that for statistical processing of the data shown in Fig. 3, where $\tau = 0$ h ($K_p$ is current index), $\Lambda_T$ for the storm growth phase will be higher than the model values due to the large delay. So the best correlation on the average will be observed if we take the averaged $K_p$ value for the previous 4.4 h. We recall that for calculation of the EBDP position $K_p$ is usually

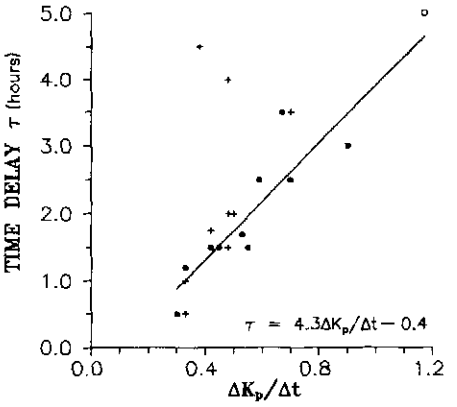


Fig. 5. Dependence of the delay time $\tau$ on the disturbance growth rate $\Delta K_p/\Delta t$ for mid-night and morning troughs obtained from the Cosmos-900 data (dots). The regression line for these conditions is shown too. For comparison, the Cosmos-900 data for the evening hours (crosses) and Ariel-3 data for 05 LT taken from the paper by Tulunay and Hughes (1973) (one open circle) are presented too.

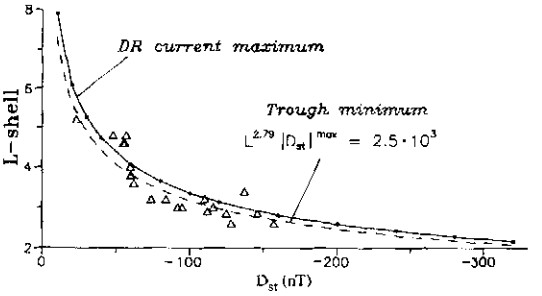


Fig. 6. Dependence of the trough position L-shell in the summer hemisphere on $D_{st}$. The ground-based data are marked by triangles, the dashed line is the best fit curve. For comparison, the position of the DR-current maximum (after Kuznetsov, 1979) is shown by the solid line with dots.

taken for the previous 3–6 h (Soloviov *et al.*, 1989). Thus, judging from the $\tau$ delay, variations in the trough minimum position and EBDP at midnight are, to a first approximation, in accordance during the storm growth phase.

### 2.5. $D_{st}$ *effects on trough position*

The main ionospheric trough is a typical feature for night-time winter conditions. However, a quite clear trough may be observed also in a summer hemisphere. This is coupled with the ring current, at least during magnetically active periods, more tightly than with the equatorward edge of auroral diffuse precipitation (Deminov *et al.*, 1992a). Indeed, in the recent studies of Besprozvannaya and co-workers (1993, 1994), a very clear connection of the trough minimum position with the ring current maximum location has been revealed. Figure 6 shows these results; dots connected by a solid line show the relationship between $D_{st}$ and the ring current maximum position, obtained from satellite data (Kuznetsov, 1979). In the previous study of Besprozvannaya and Shchuka (1993), only maxima of the main phase of 13 storms were analysed. The following approximation for the minimum position of the summer trough in $N_mF2$ was obtained:

$$L_T^{2.79}|D_{st}|^{max} = 2.5 \times 10^3 \text{ nT} \qquad (5)$$

This approximation is also shown in Fig. 6, as the dashed line, which is very similar to the curve for the the ring current but is situated somewhat lower in latitude. Thus, the maximum depletion in the F2-layer ionization is observed near the L-shell at which the ring current maximum is located. Using data from 20 ground-based stations for the SUNDIAL, September 1989 interval, Besprozvannaya *et al.* (1994) showed that expression (5) is valid not only for the storm main phase maximum but for any current state of the storm including the recovery phase. Thus, the mid-latitude trough in the summer hemisphere is tightly associated with the well-developed ring current and its position is practically entirely determined by the current value of $D_{st}$ during the storm. But its position weakly correlates with $K_p$ index; the trough seems to be not coupled with EBDP. Thus, it is rather the RIT than the MIT that is investigated. But co-ordinated observations of the trough and EBDP are required to solve this problem unambiguously.

The trough minimum position in winter and in the equinoxes correlates with $D_{st}$ weaker than with the $K_p$ index, in general, and during main phase of the storm in particular. So one may go another way: to keep the basic relationship with $K_p$ index and to try to distinguish the additional dependence on the $D_{st}$ variation. Such an analysis has been made for the main phase of the storms (for $K_p^{max}(\tau)$) when the relationship of the trough with the ring current is most evident. Deviations of the trough location from the model, which takes into account the $K_p$ index taken with a delay $\tau$, are shown in Fig. 7 (Karpachev, 1993). As the $\Delta\Lambda_T$ dependence on $D_{st}$ is expected to be not very strong and the data scatter is significant, then the correlation coefficient for the data in Fig. 7 is not very large ($r \simeq 0.71$). But the trend is seen quite clearly: at low $|D_{st}|$ values the trough is more poleward and at large $|D_{st}|$ values it is more equatorward than follows from the model for a given $K_p$ index. The deviation may be expressed by the following equation of linear

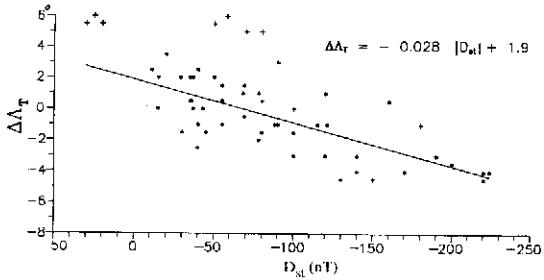


Fig. 7. Dependence of the trough minimum position (dots) on $D_{st}$. $\Delta\Lambda_T = \Lambda_T^{expr} - \Lambda_T^{mod}$, where $\Lambda_T^{expr}$ are the Cosmos-900 data and $\Lambda_T^{mod}$ are calculated for the $K_p$ index during the maximum of the storm main phase. More detail about the regression line and Cosmos-900 data (crosses) are given in the text.

regression (Karpachev, 1993): $\Delta\Lambda_T = -0.028\ |D_{st}| + 1.9$. This expression may be used for the correction of the model which only takes into account the $K_p$ index. Of course, for large values of $D_{st}$, this dependence will be non-linear. But such very strong storms are rare events –neither Cosmos-900, nor Intercosmos-19 satellites have observed storms with $|D_{st}|^{max} \geqslant 250$ nT.

When deriving the regression equation, two groups of data (marked by crosses in Fig. 7) were not taken into account. The first of these was obtained for not very intense disturbances ($K_p = 4$–5) with a weakly developed ring current. For example, $D_{st}$ was positive during almost all of the disturbance on 1–2 August 1979. These cases are strong substorms rather than storms, so they were excluded from analysis, although they do not, generally, contradict the trend obtained. The second group of data corresponds to moderate storms with $K_p$ from 6– to 7+. For such large $K_p$ values, the trough minimum is observed at latitudes of 54–58°, which is some 5–6° higher than follows from the model. On the other hand, from Fig. 6 it follows that, for $|D_{st}| = 50$–80 nT, the trough associated with the DR-current is expected to be at latitudes of 53–60°. So, in these cases we observe rather the RIT than the MIT, and the RIT position is not determined by the model in which LT and $K_p$ index are input parameters.

### 2.6. $B_y$ *and* $B_x$ *effects on trough position*

The IMF $B_y$ and $B_x$ components influence the magnetosphere and ionosphere less strongly than $B_z$, but still quite noticeably. The $B_y$ effect was revealed as the "Svalgaard–Mansurov effect" from polar station magnetogram analyses. Cowley *et al.* (1991) have shown that the $B_y$ and $B_x$ action may be described, at least qualitatively, by the simple model 'dipole plus uniform field'. According to this model, magnetic tension caused by $B_y$ results in the asymmetry of the magnetospheric convection system in relation to the noon–midnight meridian. At ionospheric heights this manifests itself as the displacement of the auroral oval as a whole in the direction of $B_y$ in the Southern hemisphere and in the opposite direction in the Northern hemisphere. The $B_x$ component influence is similar but the asymmetry is observed in relation to the dawn-dusk meridian; the auroral oval is displaced along the noon-midnight meridian. Note that due to the sector and spiral structure of the IMF, the positive direction of $B_y$ usually corresponds to negative $B_x$, and vice versa. Thus, one may separate each other only in above assumption: $B_y$ displaces the auroral oval only in the direction of the dawn-dusk meridian and $B_x$ displaces it only in the noon-midnight direction. On the basis of this assumption, Cowley *et al.* (1991) have re-analysed the data of Holzworth and Meng (1984) and separated both these effects, the oval displacement being ~2.5° under a $B_y$ change from −4 nT to +4 nT (accordingly $B_x$ from positive to negative values). It seems that just from this point of view the main ionospheric trough position dependence on $B_x$ and $B_y$ should be analysed. Such an analysis was carried out using the Intercosmos-19 data (Ben'kova *et al.*, 1989). It was found that, for $B_z > 0$, the correlation with $B_x$ is very weak but the $B_y$ effect is clearly manifested as: $\Delta\Lambda_T = -0.25B_y - 0.65$, with correlation coefficient $r = 0.66$ (see Fig. 8a). When $B_z < 0$, the relation depends on the sign of $B_y$. If $B_y$, a close correlation with $B_z$ is observed: $\Lambda_T = 0.35B_z - 0.31$, with $r = 0.81$ (see Fig. 8b). If $B_y > 0$, it is difficult to find a dependence on the IMF. Probably this could be explained that the $-B_z$ and $+B_y$ effects are opposite in relation to the auroral oval position, and so compensate one another (Nakai, 1987).

### 2.7. *Trough dynamics in different local time sectors*

The conclusions above relate to the night-time trough. But during disturbed periods a well-shaped trough in $N_mF2$ can be observed during day-time too. In Fig. 9 observations in the sub-auroral ionosphere during a strong storm 3–4 April 1979 obtained from the Intercosmos-19 satellite in three different sectors of the local time: 12–15 LT (a), 23–02 LT (b) and 19–22 LT (c) (Deminov *et al.*, 1985) are presented. The trough positions are marked by circles. The positions of the subauroral and auroral peaks of electron temperature $T_e$ are shown too (triangles). The $T_e$ enhancement is associated with the $N_e$ minimum in the trough and with the equatorward boundary of the cusp. The filled symbols relate to the Southern hemisphere and

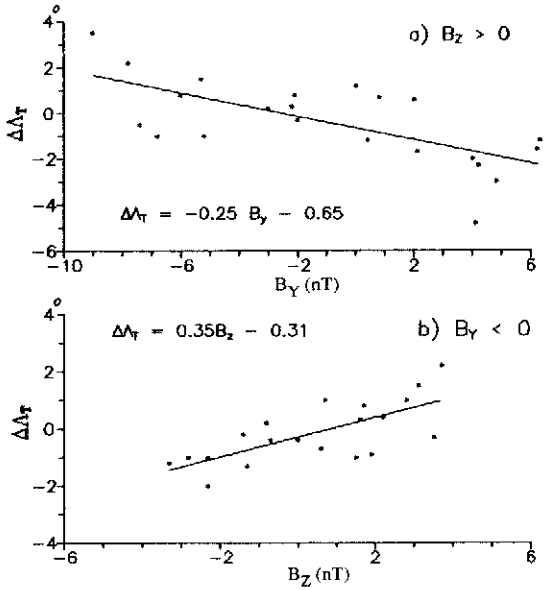


Fig. 8. Dependence of the trough minimum position on the IMF $B_y$ (a) and $B_z$ (b) components. $\Delta\Lambda_T = \Lambda_T^{exp} - \Lambda_T^{mod}$, where $\Lambda_T^{exp}$ are the Intercosmos-19 data and $\Lambda_T^{mod}$ are calculated from the model of Kohnlein and Raitt (1977).

the open symbols to the Northern hemisphere. As one could expect the day cusp (i.e. auroral peak of $T_e$) position variations correlate with the IMF $B_z$ component variations with a very small delay (Meng, 1983). This applies to the daytime trough too which is more equatorward than the cusp by several degrees. In the midnight sector (b), as was shown above, the trough position variations are determined mainly by the $K_p$ index. But the most sharp equatorward shift of the trough was observed with a time delay $\simeq 1$ h later than $B_z$ turning south. The subauroral peak of $T_e$ in this sector responds to the short-period variations of $B_z$ and a good correlation can be obtained when a time delay $\simeq 40$ min. is introduced. Finally, in the evening sector (c), the trough response as well as the $T_e$ peak to $B_z$ turning is more delayed (by $\simeq 2$ h) and is determined by the $K_p$ index variations which take into account the corresponding time delay and local time changes. More equatorward than the MIT, the $T_e$ peak for the recovery phase of the substorm (nearly 07:30 UT) corresponds to the residual ring current and is not reflected in the $N_e$ variations in the form of a density trough, as was shown in Fig. 4 (a and b).

Hence the response of the equatorial border of the auroral oval as whole and the trough minimum position to the intense geomagnetic disturbance is rather similar. The sharpest displacement of both structures towards the equator takes place almost immediately after $B_z$ turns south during daytime, and with a delay $\tau \simeq 1$ h during the night. As a result the dayside structures of the high-latitude ionosphere are controlled to a greater extent by the IMF $B_z$ component, and nighttime structures by the $K_p$ index. In the evening sector, a delay $\simeq 2$ h can be observed.

## 3. EQUATORIAL LATITUDES

The problem of the ionospheric response to IMF changes is the problem of the transfer of solar wind energy into the magnetosphere and then into the ionosphere. The high-latitude ionosphere is related to the magnetosphere by means of magnetospheric convection, electric currents and particle precipitation. Therefore the high-latitude ionospheric response to IMF changes is almost instantaneous. The largest time scale for these processes is the transport time for the hot particles from the magnetotail or from the dayside boundary layer into the auroral oval, which is no more than 1–2 h. So such a response may be called 'direct', although the solar wind energy input into the ionosphere occurs in a rather complex way. The solar wind energy may be transferred into the middle and low-latitude ionosphere, either directly from the magnetosphere in the form of electric fields and currents or indirectly through high latitudes in the form of wave disturbances and winds. Obviously, in the second case the ionosphere response will be delayed. This separation is rather relative, and the time constants for the different mechanisms of energy transfer vary continuously from about 10 min to several hours. Some aspects of the low-latitude ionospheric response to IMF changes are studied in the paper of Deminova in this issue. In this review, low latitudes will be discussed rather briefly.

### 3.1. *Response of equatorial ionosphere to variations of* $B_z$ *component*

The $f_0F2$ variations at equatorial latitudes are related to variations of the equatorial anomaly as a whole under changes of the electric field zonal component. The equatorial anomaly is very sensitive to variations of electric fields of any origin: magnetospheric convection, disturbance ionospheric dynamo and various kinds of wave disturbances. The equatorial ionospheric response to the IMF influence has been studied through the connection between equatorial and high-latitude ionospheres in various experiments in which electric fields have been measured at those latitudes (see e.g. Gonzales *et al.*, 1979). The three-dimensional current system DP-2 connects the polar and equatorial latitudes (see references in the

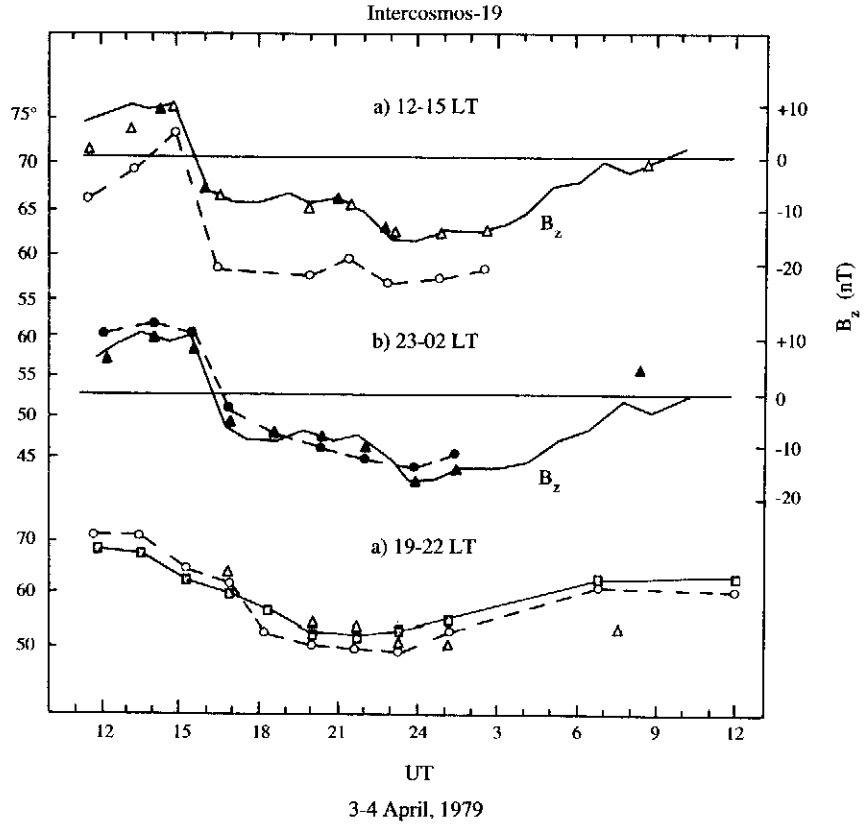


Fig. 9. Variations of the trough minimum and $T_e$ peak position in three different sectors of local time during the storm on 3–4 April 1979. Triangles are the electron temperature peaks, circles are the main ionospheric trough minimum position, open symbols correspond to the Northern hemisphere and the filled symbols to the Southern hemisphere. Variations of the IMF $B_z$ component are shown by the solid lines.

review by Matsushita, 1977). Field-aligned currents in this system are short-circuited partly through the dayside low latitude ionosphere and they form a current system in the $E$-layer which is opposite to the quiet ionospheric dynamo current system $S_q$. A link between magnetospheric and ionospheric electric fields and currents seems to be the eastward auroral electrojet. The current system DP-2 forms about 1 h after a $B_z$ southward turning, i.e. usually simultaneously with auroral activity growth, and it vanishes under a $B_z$ northward turning. As DP-2 is 'anti-$S_q$' at low latitudes, it tends to depress the equatorial anomaly. Note that during storms the equatorial anomaly is most often suppressed (see e.g. Rajaram, 1977; Abdu *et al.*, 1991). But this suppression is obtained only as a result of averaging over many storms, while in specific cases a wide variety of the equatorial anomaly behaviour is observed, depending on the superposition of various disturbing agents. Averaged values of the drift (i.e. of the electric field) at the equator were found to correlate poorly with $B_z$ averaged values. Much stronger coupling was revealed at $B_z$ steep turnings, both southward and northward. Under a $B_z$ steep southward turning the magnetospheric electric field changes to a disturbed pattern in 10–15 min, and the polarization field at the inner edge of the plasmasheath does not have time to shield the ionosphere from it. So the magnetospheric electric field directed from dawn to dusk may penetrate into the plasmasphere in about 1–2 h after a $B_z$ southward turning (see e.g. Lyatsky, 1978; Kelley *et al.*, 1979). On the night side of the Earth this field is westward during the greater part of the night, causing the additional downward plasma drift. The F-layer height drops under action of this drift, and $f_0F2$ decreases at first over the magnetic equator and then, during the second hour after the turning, at the equatorial anomaly crests, this effect is more pronounced after mid-

night and it is maximum at 03 LT (Deminov and Deminova, 1988a, 1992; Deminova, 1995). On the dayside of the Earth this field is eastward during the greater part of day, causing the additional upward plasma drift which intensifies the equatorial anomaly. However, in the daytime, the effects caused by direct penetration of the magnetospheric electric field into the low-latitude ionosphere manifest themselves less strongly than at night. This seems to be accounted for by intense ionospheric variations caused by thermospheric processes and interfering with the $B_z$ effect. When $B_z$ turns northward, then the additional magnetospheric electric field, penetrating into the plasmasphere, has the opposite direction and drives an additional upward drift of plasma at night (Kelley *et al.*, 1979). Note that $B_z$ northward turning effects on the equatorial ionosphere are more difficult to separate in pure form, because they usually occur after periods of high magnetic activity when the ionosphere is affected by various disturbing agents such as electric fields of magnetospheric origin and of the ionospheric disturbance dynamo, internal gravity waves, disturbed thermospheric winds, etc. Therefore drift and electric field data during these periods often have ambiguous interpretations (e.g. Matsushita, 1977; Fejer, 1986, 1991).

### 3.2. $B_y$ *component effect*

As mentioned above, the IMF $B_y$ component makes a magnetospheric convection system asymmetric in relation to the noon–midnight meridian, and the auroral oval, as a whole, displaces opposite to the $B_y$ direction in the Northern hemisphere and along its direction in the Southern hemisphere. The $B_y$ effect may be revealed at all latitudes, including equatorial latitudes. Under quiet conditions this effect manifests itself as the displacement of the $S_q$ system foci (Matsushita, 1977). The most complete theoretical analysis for disturbed conditions seems to have been made by Zakharov *et al.* (1989). Their calculations have shown that the magnetospheric electric field penetrating into the equatorial ionosphere under strong disturbances, when $B_z$ is steady negative and $J_\lambda \geq 10^{-6}$ A/m, is comparable in magnitude with the ionospheric dynamo field. The zonal component of the magnetospheric electric field, which essentially forms the equatorial electrojet and causes the vertical drift in the F-region, most effectively penetrates into the equatorial ionosphere in the night and morning sectors of local time. The effect depends strongly on the $B_y$ direction (see Fig. 10): the electric field zonal component $E_\lambda$ at the equator is directed opposite to the dynamo electric field for most local times under $B_y > 0$. Under $B_y < 0$,

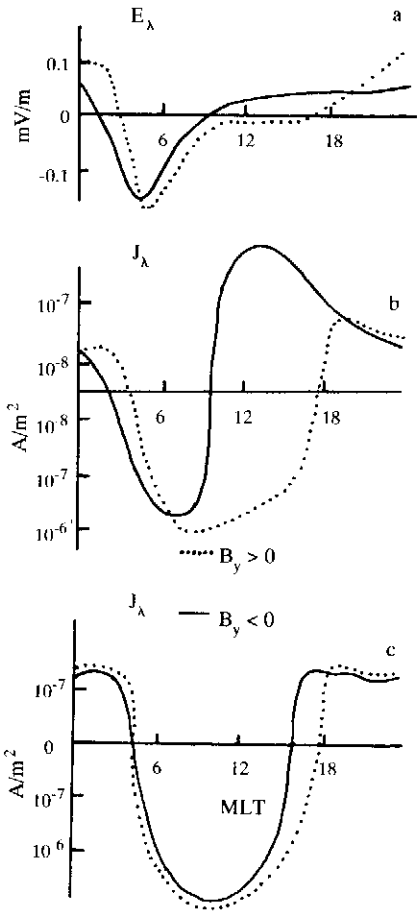


Fig. 10. Diurnal variations of the zonal component of the equatorial electric field (a) and the equatorial electrojet of magnetospheric origin: with shielding (b) and without shielding (c). Solid lines correspond to $B_z < 0$, and dotted lines to $B_z > 0$. (after Zakharov *et al.*, 1989).

the $E_\lambda$ direction coincides in phase with the dynamo field in the day and evening local time intervals and is antiphase in the other LT intervals. Fig. 10b shows variations in the density of the current in the equatorial electrojet maximum which correspond to $E_\lambda$ variations shown in Fig. 10a for the case when the magnetospheric electric field is shielded by the field-aligned currents in the plasmasheath and the auroral zone of increased conductivity. When the shielding is broken, a very strong counter-electrojet may develop which may exceed the ionospheric dynamo electrojet intensity (Fig. 10c). Such a situation may arise at the storm growth phase after a $B_z$ southward turning. Experimental evidence of magnetospheric electric field penetration into the equatorial ionosphere under $B_y$

turnings has been obtained from Cosmos-184 satellite data (Galperin *et al.*, 1978). It was shown that turnings from negative to positive $B_y$ cause an $N_i$ increase in the night-time (20–23 MLT) equatorial ionosphere, which is connected with additional upward plasma drift. Under $B_y$ turnings from positive to negative the pattern is opposite.

### 3.3. *Effects of large-scale internal gravity waves and ionospheric disturbance dynamo*

Large-scale internal gravity waves (IGW) are generated by auroral electrojet activity. Several of such bursts may occur in both hemispheres during a strong magnetospheric storm connected with a $B_z$ southward turning. As the westward and eastward electrojets are relatively independent, during the storm each of them may generate several IGWs of various amplitudes and with different time delays in relation to the storm commencement. More than 65% of strong IGWs reach the equator from both auroral ovals (Goncharova *et al.*, 1986). Each IGW has its own velocity (in the interval from 500 to 1000 m/s as a rule), and their propagation from auroral to equatorial latitudes takes different times. Therefore a very complex pattern of disturbance is observed in the equatorial ionosphere during a strong magnetic storm. An example of the IGW effect on the equatorial anomaly is shown in Fig. 11 for the 3–4 April 1979 storm as given by Intercosmos-19 satellite data (Deminov and Karpachev, 1985). The top panel in Fig. 11 shows daytime ($\sim$11 LT) effects and the lower panel relates to the night-time ($\sim$23 LT). Variations in $h_mF2$, $f_oF2$ and $f_{os}$ (plasma frequency at the satellite height $h_s \simeq 740$ km) are shown. The two curves at the bottom in Fig. 11 show variations in position of the night-time equatorial anomaly crests compared with their quiet position ($\simeq 27^\circ$ dip latitude). Positions of the day-time equatorial anomaly crests are not shown in Fig. 11 because their structure was complex and their positions could not be determined unambiguously. It is seen that in the dayside ionosphere the F-layer lifts, $N_mF2$ decreases and $N_e$ in the outer ionosphere increases 3–4 h after the eastward auroral electrojet (AU-index) enhancement. Similar effects are observed in the night-time ionosphere. The IGW effects appear 2–3 h after the enhanced AL-index (at $\simeq$17 UT) and last $\simeq$4 h. This is clearly seen from the Intercosmos-19 satellite data although the time resolution is poor. Shorter lived effects of the magnetospheric electric field ($\tau \simeq 1$–2 h) are difficult to distinguish in the Intercosmos-19 satellite data while they are clearly detected from 15-min data of ground-based stations as shown in Fig. 12. Thus, IGW cause equatorial anomaly inten-

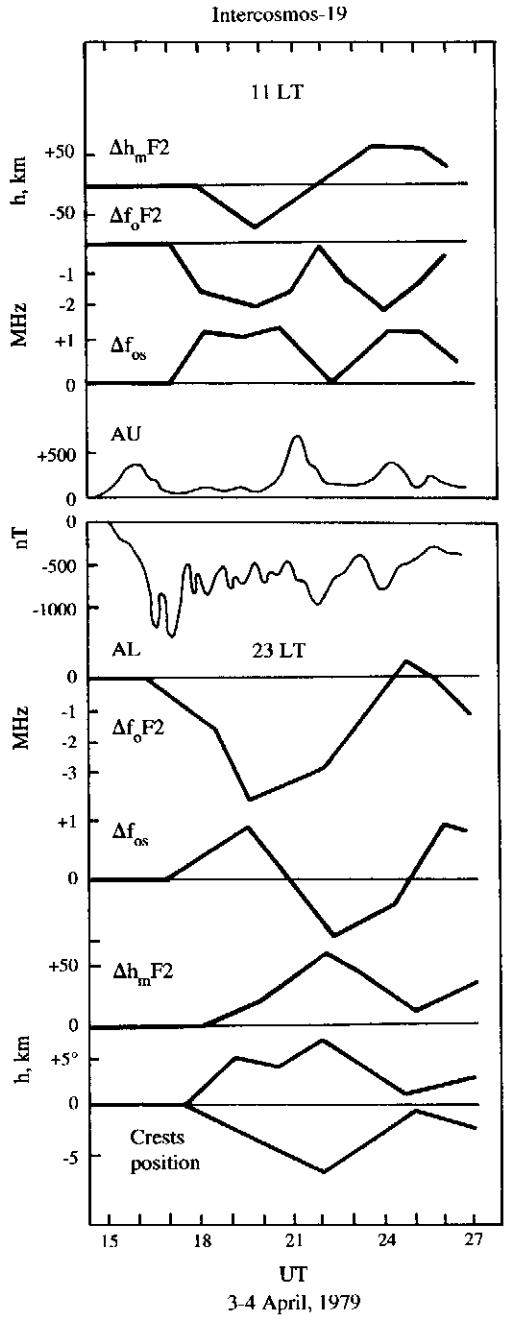


Fig. 11. Variations of $h_mF2$, $f_oF2$, $f_{os}$ (plasma frequency at the Intercosmos-19 satellite height $h_s \simeq 740$ km) above the magnetic equator during the storm on 3–4 April 1979. The variations in the latitude of the equatorial anomaly crests are also shown for the night time. The thin lines show the variations of AU and AL indices.

sification both during the day and night hours. This is connected with the complex influence of IGW on the F-layer: change of thermosphere molecular composition, wind velocity and electrodynamical plasma drift induced by IGW winds (Deminov and Deminova, 1988b).

Effects of the ionospheric dynamo have been analysed in detail by Blanc and Richmond (1980). Effects of the ionospheric disturbance dynamo at equatorial latitudes were observed by Fejer *et al.* (1983). We will not discuss their results in detail here and note only that the disturbed dynamo is driven by a vortex which is opposite to the quiet $S_q$ system (Blanc and Richmond, 1980). This begins to manifest itself at equatorial latitudes 6–8 h after auroral activity intensification associated with a $B_z$ southward turning.

### 3.4. *Concluding remarks*

Several effects in the low-latitude and equatorial ionosphere have been described which, in one way or another, are connected with the IMF. The SSC effect on $f_0F2$ may be mentioned to make the picture complete. This effect is associated with the dayside magnetosphere compression by the solar wind shock (Goncharova *et al.*, 1984). All the above effects have their own time delays in relation to the IMF change. The equatorial ionosphere seems to respond more quickly to a shock arriving at the dayside magnetosphere ($\tau \sim 10$–$15$ min) in the initial phase of a storm. Approximately 10–20 min after a $B_z$ southward turning, the electric field in the magnetotail changes, which penetrates into the plasmasphere and causes in the low-latitude ionosphere the effects described above. About 1 hour after a $B_z$ southward turning the DP-2 current system is formed, which is equivalent to an "anti-$S_q$" system at low latitudes. Auroral electrojet activity occurs on average 1 h after $B_z$ southward turnings, causing large-scale internal gravity waves which propagate from auroral to equatorial latitudes in 2–5 h and which may make strong effects in the equatorial F region (Deminov and Deminova, 1988b). The disturbed ionospheric dynamo begins to act 6–8 h after a $B_z$ southward turning in those cases when a strong magnetospheric disturbance develops after the turning. Thus, an almost continuous spectrum of time delays for different effects exists, which may be superposed on each other and build up a complex interference pattern of drifts and electric fields over the equator. For example, all the published cases of plasma drift upward turnings at night under steep and strong $B_z$ northward turnings (e.g. Patel, 1978; Fejer, 1986) occurred under more or less intense disturbances, and the effect of the large-scale IGWs, which were generated by auroral electrojet bursts several hours before the $B_z$ northward turning, interfered with the $B_z$ northward turning effect itself. This is one of the differences between the equatorial ionosphere and the polar ionosphere, where the spectrum of effects is not so broad. So, when analysing disturbances in the equatorial ionosphere, one should keep in mind the following features of the equatorial anomaly. The quiet $S_q$ current system drives an upward plasma drift over the magnetic equator at daytime, which lifts the F-layer and thus decreases $f_0F2$ over the equator and increases it at the anomaly crests. Consequently, the ionospheric disturbance dynamo, which manifests itself as 'anti-$S_q$' in the daytime (Blanc and Richmond, 1980), should create a $N_mF2$ steady increase over the equator as compared with quiet periods and this was seen in the observed data (e.g. Bremer, 1988). The DP-2 current system, which also manifests itself as 'anti-Sq' in the daytime, during disturbances (Matsushita, 1977) is consistent with model calculations (Zakharov *et al.*, 1989), from which it follows that the equatorial electrojet during a storm is weakened; it can even change its sign. It is unambiguous also that southward and northward $B_z$ turnings ought to give opposite effects in the equatorial anomaly, and this is supported by the Intercosmos-19 data (Deminov and Deminova, 1992).

## 4. MIDDLE LATITUDES

The IMF sector structure effects in the mid-latitude ionosphere were analysed by statistical methods (namely by the superposed-epoch methods) (e.g. Bremer, 1988; Tulunay, 1993). The most complete investigation has been made by Bremer (1988) who has taken into account seasonal, diurnal and solar cycle variations and the dependence on magnetic activity. He has shown that the $f_0F2$ average values under sector boundary crossings differ by no more than 0.2 MHz at any local time. Much stronger changes in $f_0F2$ are observed when the IMF $B_z$ component turns southward or northward, especially for southward turnings. This result accords to the well-known $f_0F2$ behaviour during storms: storm-time $f_0F2$ average deviations from quiet values are negative at middle latitudes, the deviation sign reverses near latitude $\sim 20^\circ$ and at the equator these deviations are positive on average. The magnitude of the effect at mid-latitudes at noon increases from $\sim 3\%$ at solar minimum to $\sim 8\%$ at solar maximum; it may reach 1 MHz in the equinoxes. This is the result of the global thermospheric circulation system, which in turn is the result of Joule heating in auroral regions. The effect

depends on season through the seasonal $B_z$ value dependence and on solar activity through the solar wind velocity (Bremer, 1988). This effect is most pronounced at dawn and weaker at dusk (Tulunay, 1993). $B_z$ southward turnings lower the mid-latitude nighttime F2-layer by $\sim 10$ km and $B_z$ northward turnings cause it to lift by approximately the same value during the first hour after the $B_z$ turning (Lyatskaya and Lyatsky, 1975). Theoretical calculations show that $B_y$ variations should influence noticeably the meridional component of the electric field, penetrating into the mid-latitude ionosphere from the magnetosphere for strong magnetospheric disturbances (Zakharov *et al.*, 1989). Bremer (1988) derived the average behaviour of $f_0$F2 at time intervals of several days. After a $B_z$ southward turning, strong variations in the mid-latitude ionospheric parameters ($f_0$F2 and $h_m$F2) occur on time scales of the order of one hour. The superposed-epoch method is not suitable for analysis of all these effects separately, and an analysis of specific cases is required. As an illustration, let us analyse the ionospheric behaviour during the strong storm on 3–4 April 1979.

We trace the effects of the storm with the help of Fig. 12 where the variations in $f_0$F2 are shown for three Japanese stations situated on the same meridian: Wakkanai ($\Lambda = 35°$), Tokyo (25°) and Okinawa (15°) (Deminov and Karpachev, 1985). The negative phase of the storm was initiated by the $B_z$ southward turning at $\approx 15$ UT. This was accompanied by the intensification of the magnetospheric convection which is seen from the change of $I_{RC}$ which indicates the rate of energy input in the ring current. Then the negative disturbance in $f_0$F2 seems to be enhanced by the IGW action at 19–20 UT. The deep negative $\Delta f_0$F2 is maintained by the reconstruction of the global thermospheric circulation system accompanied by the decrease of $O/N_2$ and consequently of $f_0$F2. The sharp increase of negative $B_z$ near 23 UT was accompanied by another increase of the magnetospheric convection electric field which reflected strongly on the $f_0$F2 variations because it occurred in the morning sector of local time for Japan. The Intercosmos-19 data analysis for this LT sector shows that $f_0$F2 variations over the Japanese stations were caused by a sharp displacement of the equatorial anomaly northern crest from $\Lambda \sim 24°$ to $\sim 19°$. One can see also that for the entire observational period the small-scale variations at Wakkanai (35°) correlate with corresponding variations of the horizontal component of the terrestrial magnetic field at nearby Kakkioka (34°). It is a manifestation of the ionospheric dynamo electric field created by neutral wind variations. We can separate the $f_0$F2 variations caused by the Travelling Ionospheric

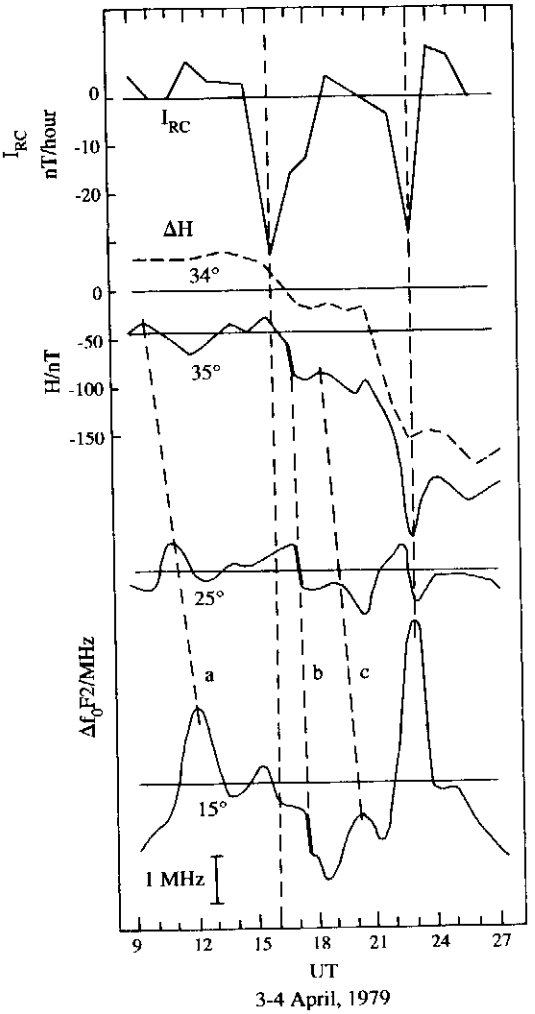


Fig. 12. Variations of $I_{RC}$ (the growth rate of DR-current), $\Delta H$ (horizontal component of the geomagnetic field at Kakkioka) and $f_0$F2 at Wakkanai ($\Lambda = 35°$), Tokyo (25°) and Okinawa (15°) during the storm on 3–4 April 1979. Travelling Ionospheric Disturbances are marked by a, b and c.

Disturbances labelled by a, b and c in Fig. 12 caused by IGWs generated by the auroral electrojet (which could be seen from the AE-index variations) and the MHD wave which appeared in the form of a sharpening of the IGW front. This is connected with the moment of first intensification of the magnetospheric convection electric field ($\approx 16$ UT).

So the $B_z$ control of the ionosphere has a global character and is shown through the indices of geomagnetic activity. This makes it possible to construct a schematic picture of the global response of the upper

ionosphere to the strong geomagnetic disturbance caused by the sharp turning of the $B_z$ to the south.

## 5. PATTERN OF GLOBAL IONOSPHERIC RESPONSE TO GEOMAGNETIC DISTURBANCE

We have described above the main features of the changes to the high, low and middle latitude ionosphere. Now we try to combine all of them into a general picture of the global ionospheric response to the strong geomagnetic disturbance caused by $B_z$ turning to the south, using the 3–4 April 1979 storm. In Fig. 13, the pattern of disturbance ($\Delta f_0F2$) development is shown for the local night sector (21-01 LT), constructed with respect to the longitudinal effect in $f_0F2$ (Deminov and Karpachev, 1988; Karpachev, 1988). The equatorial anomaly variations are shown in terms of dip latitude, and the main trough variations in terms of invariant latitude. The high-latitude part of the map with the trough and its low-latitude part with the equatorial anomaly are joined together along the 40° INV LAT which approximately corresponds to ±60° DIP LAT.

The magnetospheric storm began at 10.02 UT after a SSC. At the initial phase of the ionospheric storm a well developed positive disturbance (up to +3 MHz in the Northern hemisphere) is observed in the region of the trough equatorward wall. With the beginning of the main phase of the storm, after the $B_z$ turning, the trough begins to move towards the equator. This movement depends on local time; at the latitude of the trough's poleward wall one can observe the strong deviation in $f_0F2$ from the undisturbed level and, at the latitudes of the equatorward wall of the trough, the negative variations in $f_0F2$ are related to the trough minimum movement and the negative phase development at the middle latitudes. The equatorial anomaly response consists of two parts: inhibition of the equatorial anomaly 1–2 h after the $B_z$ turning related to downward drift, and development of the equatorial anomaly under IGW effects reaching the equator 2–5 h after the burst of the westward electrojet which is also associated with the $B_z$ turning. The weakening of the equatorial anomaly manifests itself most clearly at ~03 LT; this is not observed by the Intercosmos-19 satellite data shown in Fig. 13. During the equatorial anomaly intensification $f_0F2$ decreases over the magnetic equator and increases at the equatorial anomaly crests, and the equatorial anomaly crests move away from the equator.

One can see that the variations in $f_0F2$ related to the trough and equatorial anomaly movements cover all the ionosphere, including middle latitudes. Therefore the changes of the $f_0F2$ values through the main phase of the storm is determined mainly by variations at high and low latitudes and by the development of strong negative variations at middle latitudes.

## 6. CONCLUSIONS

We have tried to construct a global picture of the ionosphere response to the intensive magnetic disturbance connected with IMF variations. The main features are as follows:

Variations of $f_0F2$ during the main phase of a strong storm, associated with the $B_z$ turning southwards, are determined mainly by the variations in the high-latitude and equatorial ionosphere, accompanied by the decrease at middle latitudes;

Variations of the equatorial boundary of the auroral oval and of the trough minimum position are correlated: the largest displacement towards the equator takes place immediately after the $B_z$ turning to the south in daytime hours, and with a delay of 1–1.5 h at night. In the evening the delay could reach 2 h. All this is expressed by the better correlation with $B_z$ in the day-time and with $K_p$ index at night;

The response of the mid-latitude trough to the $K_p$ index variations is described by a time lag $\tau$ during all phases of the storm. The delay time $\tau$ for the growth phase of the storm depends on the disturbance growth rate: $\tau = 4.3\Delta K_p/\Delta t - 0.4$ h. On average $\tau \approx 2.2$ h, so the best correlation will be obtained for $K_p$ averaged for preceding ≈4.4 h;

Short-period variations in the night-time winter trough position (up to ±4° in latitude) are determined by the additional effects of $D_{st}$, $B_y$ and $B_z$ (all in nT). In addition, under $B_z > 0$, a good correlation is observed with the value of $B_y$: $\Delta\Lambda_T = -0.25B_y - 0.65$ and, for $B_y < 0$, correlation with $B_z$ is observed: $\Delta\Lambda_T = 0.35B_z - 0.31$. Dependence on $D_{st}$ is presented in a linear approximation too: $\Delta\Lambda_T = -0.028|D_{st}| + 1.9$;

In the summer hemisphere the nightside trough position correlates with $D_{st}$ better than with $K_p$ index. This connection may be represented in the following form: $L_T^{2.79}|D_{st}|^{max} = 2.5 \times 10^3$ nT;

For the recovery phase of the storm, often (especially in the morning hours) an additional trough is observed which is situated equatorward of the MIT, which is called the ring ionospheric trough (RIT). The RIT position practically does not depend on the $K_p$ index and tends to the latitude of the residual ring current. When both troughs are situated close in latitude the RIT could mask the MIT, which causes complexity in the analysis of subauroral ionospheric behaviour;

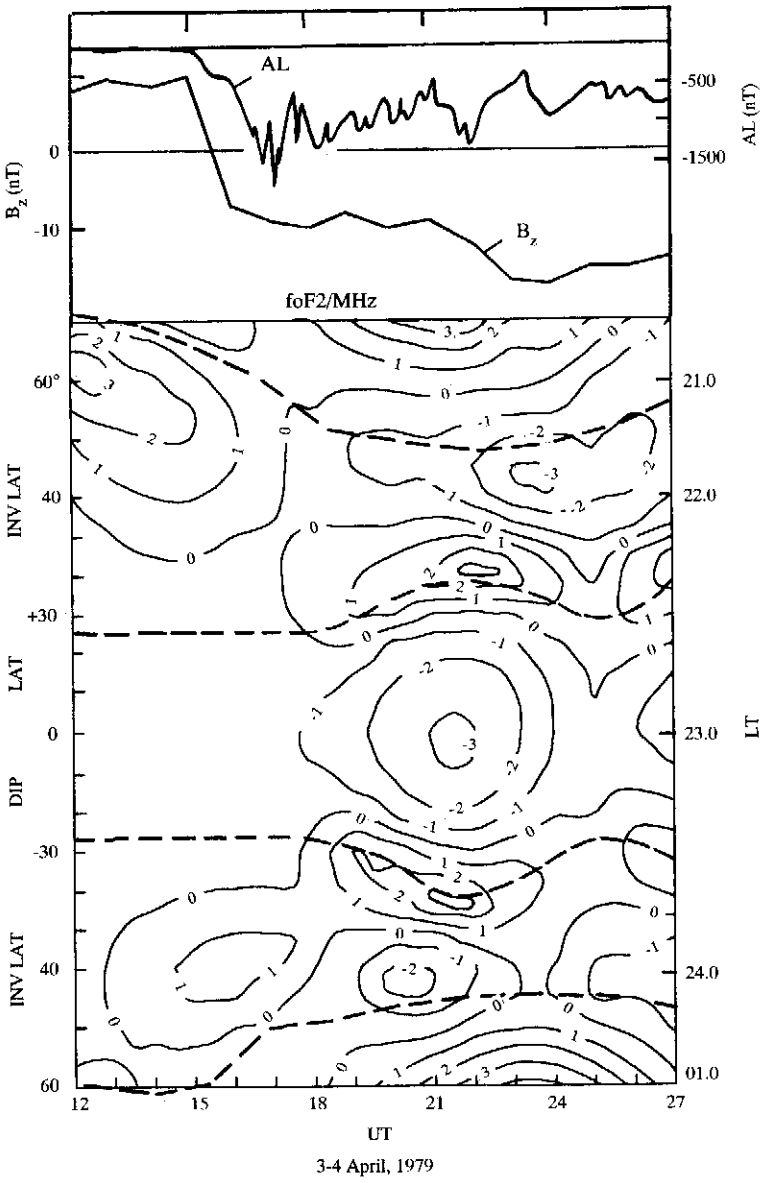


Fig. 13. Schematic pattern of the $f_0F2$ global response to the strong magnetic storm on 3 4 April 1979 from the Intercosmos-19 satellite data. Top panel: variations of $B_z$ and AL index. Bottom panel: variations in $f_0F2$ (solid lines) and positions of the trough minimum and equatorial anomaly crests (dashed lines). The high-latitude part of the map is presented versus INV LAT, and the low-latitude part versus DIP LAT.

At equatorial latitudes a $B_z$ southward turning causes additional downward plasma drift on the night-side of the Earth, which leads to the equatorial anomaly weakening, and the upward drift on the day side which intensifies the equatorial anomaly. Large-scale IGWs reaching the equator 2 5 h after auroral electrojet activity cause the equatorial anomaly intensification. The superposition of all these effects gives rise to very complex variations;

The middle latitude ionospheric variations during

geomagnetic disturbances have probably the most complex character because they are determined practically by all the factors taking place during the storm: the high latitude and low latitude ionosphere variations, effects of electric fields of both magnetospheric and ionospheric origin, wave disturbances, negative changes connected with the global circulation system, etc.

In conclusion we mention that the accuracy of the disturbed ionosphere analysis depends on an accurate knowledge of the quiet ionospheric state. It is possible to show that if we do not take into account the longitudinal effect at equatorial latitudes we obtain not only incorrect values of the $f_0F2$ variation but also the wrong sign. This work is based on the studies of the background state of the ionosphere by Deminov and Karpachev (1988) and Karpachev (1988, 1992). Finally, a model of the MIT taking into account the trough position dependence on longitude, latitude, height, local time, $K_p$ index and season is now close to completion.

## REFERENCES


Abdu M. A., Sobral J. H. A., de Paula E. R. and Batista I. S. 1991 Magnetospheric disturbance effects on the Equatorial Ionization Anomaly (EIA): an overview. *J. atmos. terr. Phys.* **53,** 757–771.

Afonin V. V., Deminov M. G., Karpachev A. T., Ben'kova N. P., Besprozvannaya A. S., Shestakova L. V., Shmilauer Ya. and Shchuka T. I. 1992 The longitude variations of the main ionospheric trough position during the night-time winter condition according to the Cosmos-900 and Intercosmos-19 satellites date. *Geomagnetism and Aeronomy* **32,** N2, 75–78.

Ben'kova N. P., Besprozvannaya A. S., Kozlov E. F., Kochenova N. A., Samorokin N. I. and Shchuka T. I. 1989 The effect of IMF on the main ionospheric trough position according to the Intercosmos-19 satellite data. *Geomagnetism and Aeronomy* **29,** 863–865.

Besprozvannaya A. S. and Shchuka T. I. 1993 Dynamics of the main ionospheric trough during the global storms with the intense ring current. *Geomagnetism and Aeronomy* **33,** N6, 145–150.

Besprozvannaya A. S., Shchuka T. I., Kishcha P. V., Nepomnyashchkaya E. V. and Pulinds S. A. 1994 DR-current effects on the trough dynamics. Model and experimental data comparison for the SUNDIAL September 1989 interval. *Geomagnetism and Aeronomy* **34,** 166–169.

Blanc M. and Richmond A. D. 1980 The ionospheric disturbance dynamo. *J. Geophys. Res.* **80,** 1669–1686.

Brautigam D. H., Gussenhoven M. S. and Hardy D. A. 1991 A statistical study on the effect of IMF $B_z$ and solar wind speed on auroral ion and electron precipitation. *J. Geophys. Res.* **96,** 5525–5538.

Bremer J. 1988 The influence of the IMF structure on the ionospheric F-region *J. atmos. terr. Phys.* **50,** 831–838.

Burton R. K., McPherron R. L. and Russel C. T. 1975 An empirical relationship between interplanetary conditions and $D_{st}$. *J. Geophys. Res.* **80,** 4204–4214.

Carbary J. F. and Meng C.-I. 1988 Correlation of the cusp with AE(12) and $B_z$. *Planet. Space Sci.* **36,** 157–161.

Cowley S. W. H., Morelli J. P. and Lockwood M. 1991 Dependence of convective flows and particle precipitation in the high-latitude dayside ionosphere on the $X$ and $Y$ components of the interplanetary magnetic field. *J. Geophys. Res.* **96,** 1557–1564.

Deminov M. G., Karpachev A. T., Kushnerevsky Yu. V. and Shmilauer Ya. 1985 The structure of the subauroral ionosphere during the magnetospheric storm according to the Intercosmos-19 satellite data. *Geomagnetism and Aeronomy* **25,** 406–409.

Deminov M. G. and Karpachev A. T. 1985 Response of the ionosphere on the magnetospheric storm. *Forecasting of the Ionosphere and Radio Wave Propagation Conditions*, Nauka publ., Moscow, 68–77.

Deminov M. G. and Karpachev A. T. 1986 The longitudinal effect in the main ionospheric trough configuration. I. The trough position. *Geomagnetism and Aeronomy* **26,** 63–68.

Deminov M. G. and Karpachev A. T. 1988 Longitudinal effect in the night-time mid-latitude ionosphere from the Intercosmos-19 satellite data. *Geomagnetism and Aeronomy* **28,** 76–80.

| | | |
|---|---|---|
| Deminov M. G. and Deminova G. F. | 1988a | Electric field in the night-time equatorial ionosphere at southward turning of the IMF $B_z$-component. *Geomagnetism and Aeronomy* **28,** 319–321. |
| Deminov M. G. and Deminova G. F. | 1988b | Ionospheric effects of AGW over the geomagnetic equator. *Geomagnetism and Aeronomy* **28,** 219–222. |
| Deminov M. G. and Deminova G. F. | 1992 | Response of the night-time low-latitudinal ionosphere to the IMF $B_z$ turnings according to the Intercosmos-19 satellite data. *Geomagnetism and Aeronomy* **32,** N3, 10–15. |
| Deminov M. G., Karpachev A. T. and Morozova L. P. | 1992a | The subauroral ionosphere during SUNDIAL period, June 1987, according to the data of Cosmos-1809 satellite. *Geomagnetism and Aeronomy* **32,** N1, 54–58. |
| Deminov M. G., Karpachev A. T., Afonin V. V., and Shmilauer Ya. | 1992b | The variations of the main ionospheric trough position along the longitude and geomagnetic activity. *Geomagnetism and Aeronomy* **32,** N5, 185–188. |
| Deminov M. G., Karpachev A. T., Afonin V. V., Anna Kuliev S. K. and Shmilauer Ya. | 1993 | Dynamics of the mid-latitude ionospheric trough during the storms. I. Qualitative pattern. *Geomagnetism and Aeronomy* **35,** 73–79. |
| Fejer B. G., Larsen M. F. and Farley D. T. | 1983 | Equatorial disturbance dynamo electric fields. *Geophys. Res. Lett.* **10,** 537–540. |
| Fejer B. G. | 1986 | Equatorial ionospheric fields associated with magnetospheric disturbances. In: *Solar Wind-Magnetosphere Coupling*, TERRAPUB/Reidel, Tokyo, 519–545. |
| Fejer B. G. | 1991 | Low latitude electrodynamic plasma drifts: a review. *J. atmos. terr. Phys.* **53,** 677–693. |
| Fok M.-C., Kozyra J. U., Warren M. F. and Brace L. H. | 1991 | Seasonal variations in the subauroral electron temperature enhancement. *J. Geophys. Res.* **96,** 9773–9780. |
| Galperin Yu. I., Ponomarev V. N. and Zosimova A. G. | 1973 | *In-situ* measurements of ion drift velosity in the upper ionosphere during a magnetic storm. *Kosmicheskie issledovaniya* **11,** 284–296. |
| Galperin Yu. I., Ponomarev V. N. and Zosimova A. G. | 1978 | Equatorial ionospheric anomaly and interplanetary magnetic field. *J. Geophys. Res.* **83,** 4265–4271. |
| Goncharova E. E., Deminov M. G., Pushkova G. N. and Yudovich L. A. | 1984 | Electric field of the substorm at the mid-latitudes. *Ionosphere-magnetosphere Disturbances and their Forecasting*, Nauka publ., Moscow, 62–65. |
| Goncharova E. E., Deminova G. F., Shashunkina V. M. and Yudovich L. A. | 1986 | Empirical model of ionospheric effect of internal gravity waves for low and equatorial latitudes. *Ionospheric Studies USSR Academy of Sciences* **41,** 109–114. |
| Gonzales C. A., Kelley M. C., Fejer B. G., Vickery J. F. and Woodman R. F. | 1979 | Equatorial electric fields during magnetically disturbed conditions. 2. Implication of simultaneous auroral and equatorial measurements. *J. Geophys. Res.* **84,** 5803–5812. |
| Holzworth R. H. and Meng C.-I. | 1984 | Auroral boundary variations and the interplanetary magnetic field. *Planet. Space Sci.* **32,** 25–29. |
| Kamide Y. and Winningham J. D. | 1977 | A statistical study of the "instantaneous" nightside auroral oval: the equatorward boundary of electron precipitation as observed by ISIS 1 and 2 satellites. *J. Geophys. Res.* **82,** 5573–5588. |
| Karpachev A. T. | 1988 | The features of the global longitudinal effect in the night-time equatorial anomaly. *Geomagnetism and Aeronomy* **28,** 46–49. |
| Karpachev A. T. | 1992 | Global variations of foF2 in the night-time ionospheric trough region. *Geomagnetism and Aeronomy* **32,** N5, 94–98. |
| Karpachev A. T. | 1993 | Private communication. |
| Karpachev A. T., Afonin V. V. and Smilauer Ya. | 1994 | The variations of the night-time trough position along longitude during winter and equinox: a comparison. *Geomagnetism and Aeronomy* **34,** 70–75. |
| Kelley M. C., Fejer B. G. and Gonzalez C. A. | 1979 | An explanation for anomalous equatorial ionospheric electric fields associated with a northward turning of the interplanetary magnetic field. *Geophys. Res. Lett.* **6,** 301–304. |

Khalipov V. L., Sivtseva L. D., Filippov V. M., Nikolaenko L. M., Stepanov A. E. and Bosqued J. M. 1985 Step-like profiles of electron density in the subauroral lower F-region in the morning sector and possible mechanisms of their formation during substorm: the comparison of data of ground-based ionosondes with the AUREOL-3 satellite measurements. *Results of the ARCAD 3 PROJECT*. Toulouse-84, Cepadues-editions, 219–232.

Kohnlein W. and Raitt W. J. 1977 Position of the mid-latitude trough in the topside ionosphere as deduced from ESRO-4 observations. *Planet. Space Sci.* **25,** 600–602.

Kuznetsov S. I. 1979 $D_{st}$ variation as the measure of the some phenomenon in the inner magnetosphere. *Symposium of KAPG on the Solar-Terrestrial Physics*. Ashkhabad, 1976, Abstracts, 57.

Lyatsky V. B. 1978 Systems of currents during magnetospheric-ionospheric disturbances. Leningrad, Nauka publishing, 1978.

Lyatskaya A. M. and Lyatsky V. B. 1975 Magnetic field of solar wind and vertical movement of the night ionosphere. *Geomagnetism and Aeronomy* **15,** 977–981.

Makita K., Meng C.-I. and Akasofu S.-I. 1985 Temporal and spatial variations of the polar cap dimension inferred from the precipitation boundaries. *J. Geophys. Res.* **90,** 2744–2752.

Matsushita S. 1977 IMFP effects on the equatorial geomagnetic field and ionosphere—a review. *J. atmos. terr. Phys.* **39,** 1207–1215.

Meng C.-I. 1979 Diurnal variations of the auroral oval size. *J. Geophys. Res.* **84,** 5319–5324.

Meng C.-I. 1983 Case studies of the storm time variations of the polar cusp. *J. Geophys. Res.* **88,** 137–149.

Nakai H. 1987 The northern and southern auroral ovals in response to the IMF $B_y$-component. *Geophys. Res. Lett.*, **14,** 1162–1165.

Nakai H. and Kamide Y. 1983 Response of nightside auroral oval boundaries to the interplanetary magnetic field. *J. Geophys. Res.* **88,** 4005–4014.

Nakai H., Kamide Y., Hardy D. A. and Gussenhoven M. S. 1986 Time scales of expansion and contraction of auroral oval. *J. Geophys. Res.* **91,** 4437–4450.

Patel V. L. 1978 Interplanetary magnetic field variations and the electromagnetic state of the equatorial ionosphere. *J. Geophys. Res.* **83,** 2137–2144.

Rajaram G. 1977 Structure of the equatorial F-region, topside and bottomside—a review. *J. atmos. terr. Phys.* **39,** 1125–1144.

Rodger A. S., Brace L. H., Hoegy W. R. and Winningham J. D. 1986 The poleward edge of the mid-latitude trough—its formation, orientation and dynamics. *J. atmos. terr. Phys.* **48,** 715–728.

Soloviov V. S., Galperin Yu. I. and Zinin L. V. 1989 Diffuse auroral zone. IX. Equatorial border of the diffuse precipitations of the plasma sheet electrons as the border of the convection in the magnetosphere (plasmapause). *Kosmicheskie issledovaniya* **27,** 232–247.

Spiro R. W., Heelis R. A. and Hauson W. B. 1979 Rapid subauroral ion drifts observed by Atmospheric Explorer C. *Geophys. Res. Lett.* **6,** 657–660.

Tsurutani B. T., Goldstein B. E. *et al.* 1990 The interplanetary and solar causes of geomagnetic activity. *Planet. Space Sci.* **38,** 109–126.

Tulunay Y. and Hughes A. R. W. 1973 A satellite study of the mid-latitude trough in electron density and VLF radio emissions during the magnetic storm 25–27 May 1967. *J. atm. terr. Phys.* **35,** 153–163.

Tulunay Y. 1993 Interplanetary magnetic field and its possible effects on the mid-latitude ionosphere. 2. URSI/PRIME Workshop, Graz, Report, 1–4.

Zakharov V. E., Nikitin M. A. and Smirnov O. A. 1989 The response of low-latitude electric field to the action of magnetic source. *Geomagnetism and Aeronomy* **29,** 381–388.